Ministry of Science, Research & Technology
Iranian Research Organization for Science and Technology (IROST)

Journal of PARTICLE Science & Technology

JPSIT

https://jpst.irost.ir

Research paper

Synthesis, characterization, and magnetic properties of $NiFe_2O_4$ nanoparticles

Sayed Ali Hassanzadeh-Tabrizi

Advanced Materials Research Center, Department of Materials Engineering, Najafabad Branch, Islamic Azad University, Najafabad, Iran

HIGHLIGHTS

- $NiFe_2O_4$ was prepared via a polyacrylamide gel method.
- A crystalline $NiFe_2O_4$ phase with a cubic structure is produced.
- The crystallite size increases with increasing calcination temperature, whereas the lattice strain slumps.
- The activation energy for crystallite growth was calculated to be 43.2 $KJ.mol^{-1}$.

GRAPHICAL ABSTRACT

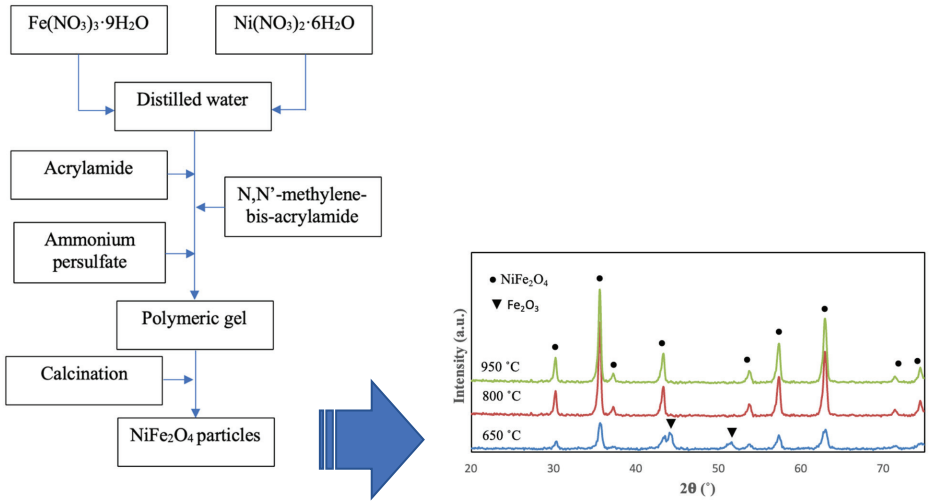

ARTICLE INFO

Article history:

Received 2 January 2023
Revised 15 January 2023
Accepted 9 February 2023

Keywords:

$NiFe_2O_4$
Polyacrylamide gel
Magnetic properties
Nanomaterials

ABSTRACT

In order to adjust the crystallite size and structure, $NiFe_2O_4$ was prepared in this study via a polyacrylamide gel method. Various characterization techniques like XRD, FT-IR, SEM, and VSM were used to learn more about the fabricated materials. The XRD corroborated that a crystalline $NiFe_2O_4$ phase with a cubic structure was produced. Microstructural studies showed that the produced particles have an irregular morphology with an average particle size of about 90 nm. The Williamson-Hall equation was utilized to examine the contributions of crystallite size and lattice strain of the samples. STA results showed the decomposition of the polymeric network gel during calcination. The crystallite size increases with increasing calcination temperatures, whereas the lattice strain slumps. The activation energy for crystallite growth was calculated to be 43.2 $KJ.mol^{-1}$. VSM findings showed that saturation magnetization improves with temperature, which may be attributed to the crystallite growth of the particles. The coercivity of the samples dropped with an increase in the temperature.

DOI: 10.22104/JPST.2023.6046.1220

** Corresponding author: Tel.: +9831-42292893 ; Fax: +9831-42291016 ; E-mail address: hassanzadeh@pmt.iaun.ac.ir*

1. Introduction

Cubic magnetic ferrite with a general formula of MFe_2O_4, where M is a divalent cation, has drawn immense attention due to its magnetic properties and numerous applications in the different sectors of technology, biomedicine, catalysis, and the environment [1]. Nickel ferrite ($NiFe_2O_4$) nanoparticles, which are among the spinel ferrites, have captured researchers' attention in a number of fields, including catalysis, sensing, and photocatalysis [2,3]. Because of its unique magnetic and electric properties, this material is regarded as one of the most important soft magnets. In this ferrite, Fe^{3+} is found in the tetrahedral area, whereas Fe^{3+} and Ni^{2+} are found in the octahedral area, and it exists as an inverse spinel structure [4].

The synthesis method greatly affects the quality of the final fabricated product [5]. Magnetic ferrites powders are traditionally fabricated through a solid-state reaction by mixing their oxide components [6]. The mixtures are milled, and then the milled mixtures are subjected to heat for a long period at high temperatures to reach pure ferrites and remove unwanted intermediate phases [7]. Creating ferrites powders via the solid-state reaction approach is a relatively easy process. However, during ball milling, it is inevitable that certain contaminants may be incorporated. Additionally, considerable large grain development and rigid agglomerates are produced by prolonged high-temperature heat treatment. [8] Numerous wet chemical processes have been recently developed to create ferrite powders, including co-precipitation [9], microwave-hydrothermal [10], auto-combustion [11], sol-gel [12], radio-frequency thermal plasma torch [13], organic acid precursor [14], and other methods. The polyacrylamide sol-gel technique is a straightforward, quick, and affordable method that can be used to fabricate ceramic powders [15]. This process produces very fine and highly dispersed powders by directly pyrolyzing the polymeric network [16]. Since aqueous solutions of inorganic salts are the original materials utilized in the polyacrylamide gel method, this enables the avoidance of pricey metal alkoxide, unlike other sol-gel techniques.

In the present study, $NiFe_2O_4$ nanoparticles were fabricated via a polyacrylamide gel method. The products were then characterized by different analytical methods. Finally, the magnetic characteristics of the synthesized nickel ferrites nanoparticles were studied.

2. Experimental

$Fe(NO_3)_3 \cdot 9H_2O$ (iron nitrate nonahydrate) and $Ni(NO_3)_2 \cdot 6H_2O$ (nickel nitrate hexahydrate) were used as crude materials for the fabrication of nickel ferrite. For the preparation of the polymeric network, acrylamide, N,N'-methylene-bis-acrylamide, and ammonium persulfate were used as starting materials. First, 0.04 mol of nickel nitrate hexahydrate and 0.08 mol of iron nitrate nonahydrate were dissolved in 400 ml of distilled water. Then, ammonium persulfate, acrylamide, and N,N'-methylene-bis-acrylamide with a mole ratio of 1/24/2 were added to the metal salt solution. After mixing the solution for 60 min, the mixture was heated to 80 °C. The heat turned the solution into a gel. Finally, the product was dried in an oven and calcined at 650, 800, and 950 °C for 3 h. Fig. 1 shows a schematic illustration of the polyacrylamide gel synthesis of $NiFe_2O_4$.

Using an AVATAR Thermo spectrometer, the Fourier transform infrared (FT-IR) spectroscopy of samples was taken. A simultaneous thermal analyzer (STA) was used to perform the differential thermal analysis (DTA) measurements and thermogravimetric analysis (TGA) of samples (BAHR- Model: STA 503). The phase compositions of specimens were evaluated with an x-ray diffraction instrument (Philips PW3040) using an X-ray tube with a copper target. Morphological

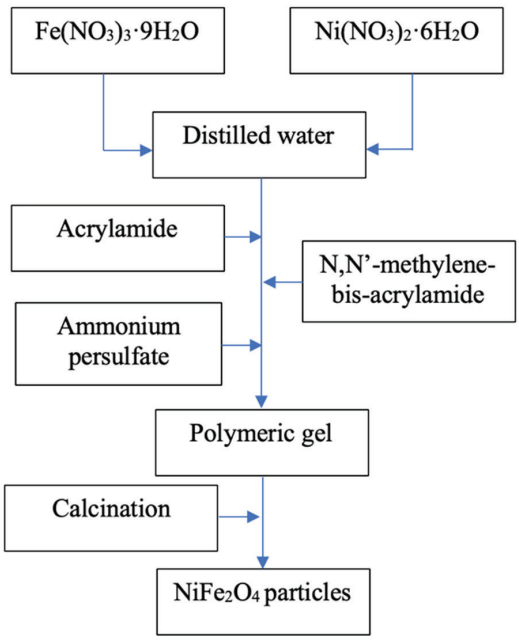

Fig. 1. Schematic illustration of the polyacrylamide gel synthesis of $NiFe_2O_4$.

studies were made via scanning electron microscopy (SEM, VEGA//TESCAN Mira 3-XMU). Magnetic characteristics of the fabricated nickel ferrite particles were attained using a vibrating sample magnetometer (VSM HH-15).

3. Results and discussion

Fig. 2 displays the FTIR spectra of the samples and their functional groups before and after calcination at 800 °C. As seen in the figure, in the pre-calcination sample, the stretching and bending vibrations of the O–H bond of water are observed at a wavenumber of 3432 and 1595 cm^{-1}, respectively [17]. The N–H bond stretching vibration is associated with the band at 3196 cm^{-1} [18]. The peak that appeared at 1640 cm^{-1} is related to the stretching vibration of an amide group. The stretching vibration of C–H bonds is responsible for the peaks at 2933 and 2858 cm^{-1} [18,19]. The absorption bands at 1029 cm^{-1}, 1401 cm^{-1}, and 1665 cm^{-1} are pertinent to C–N (stretching), N–O (stretching), and C=O (stretching) vibrations, respectively [20]. As can be seen, these peaks disappeared somewhat after the calcination, which shows the removal of volatile components and the destruction of the polymeric network. The existence of the peaks related to water after calcination is due to water the samples adsorbed from the atmosphere before the FT-IR test and is not related to the structural water. Moreover, Fe–O groups in the octahedral position and Ni–O groups in the tetrahedral position in the $NiFe_2O_4$ structure have stretching bonds that are seen at 474 and 570 cm^{-1}, respectively, that corroborate the formation of a spinel structure [21].

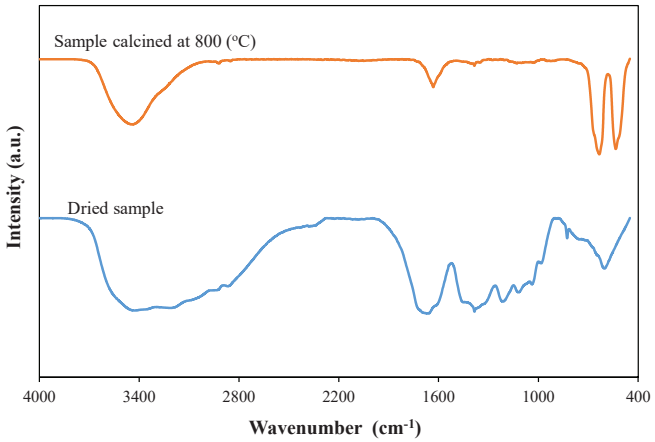

Fig. 2. FT-IR spectra of the samples before and after calcination at 800 °C.

Fig. 3 displays the thermal analysis (TG) curves for the dried sample. It can be said that the exothermic peak at about 365 °C, which pertains to a weight decline of 40 %, is connected to the decomposition of nitrate metal salts in the products and the removal of water. The degradation of the polyacrylamide's backbone and other residues is responsible for the significant exothermic peak at about 613 °C. The TG curve shows three stages of weight decline. The first drop in weight occurring between ambient temperature and 230 °C corresponds to a mass loss of 20 % and is attributed to water that has been chemically and physically adsorbed. The second weight loss between 220 °C and 410 °C is due to nitrate species decomposition. The third loss is due to the destruction of the polymeric structure of polyacrylamide, which happened at 613 °C. The TG curve shows no more weight loss after 650 °C, showing that the organic and volatile components were totally eliminated. There was a total weight decline of 88% in the sample.

The XRD results of powders calcined at different temperatures are represented in Fig. 4. As can be seen, the sample calcined at 650 °C has peaks that match card number JCPDS No. 54-0964 and confirm the formation of nickel ferrites. In addition, some peaks detected in this sample which are related to the unreacted iron oxide. In the samples calcined at higher temperatures, the peaks related to iron oxide disappear, which shows a complete reaction of raw materials and the creation of nickel ferrite.

Moreover, the intensity of the peaks increases, which corroborates the increase in the crystallinity of the samples. These findings confirm that all of these peaks can be fully suited by a cubic spinel structure. As can be seen, the nickel ferrite has been successfully synthesized without unreacted phases after calcination

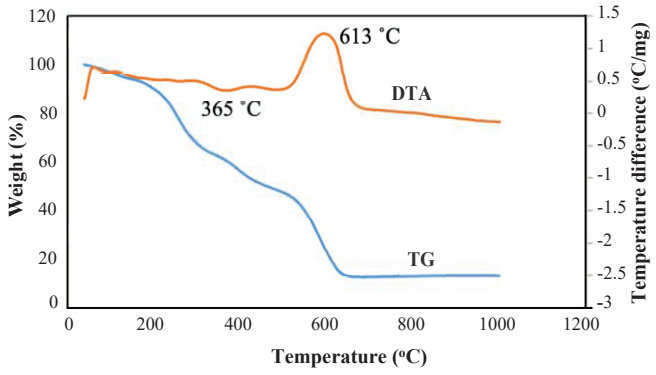

Fig. 3. The thermal analysis curves for the dried sample.

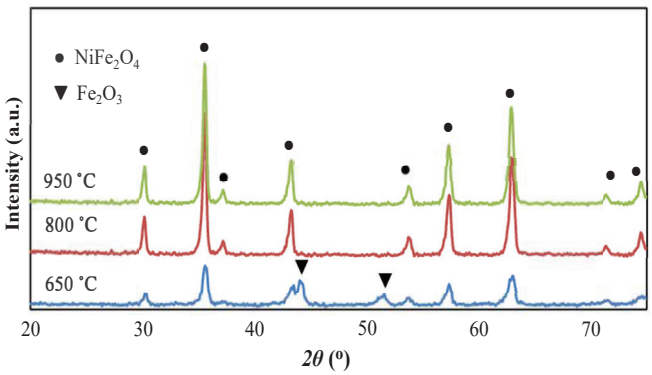

Fig. 4. XRD patterns of the heat-treated specimens at various temperatures.

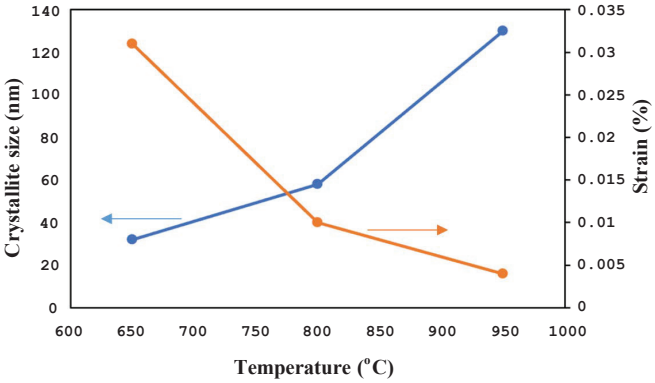

Fig. 5. Lattice strain and crystallite size of the specimens at various temperatures.

at 800 °C, which is attributed to the mixing of raw materials at the molecular level, characteristic of wet chemical methods like the polyacrylamide gel method. The mechanism of synthesis in this method can be explained as follows. First, the nickel nitrate and iron nitrate salts are dissolved in water, producing iron and nickel ions. Then, free radicals provided by persulfates can start the polymerization of the acrylamide and N,N'-methylene-bis-acrylamide, resulting in a complicated three-dimensional network with interconnected loops and branches. The polymer network offers a structural foundation for the development of nanoparticles, which can immobilize the precursor particles and so curb the nanoparticles from aggregating and growing the grains. The Williamson-Hall equation (Eq. (1), [22]) was used to investigate the crystallite size (D) and strain (ε) of the nanoparticles.

$$FWHM \cos\theta = (K\lambda/D) + 4\varepsilon \sin\theta \quad (1)$$

where λ is the wavelength, $FWHM$ is the full width at half maximum of the diffraction peaks in radians, and θ is the angle of diffractions in degrees. The results from Eq. (1) are shown in Fig. 5. As can be seen, as the calcination temperatures of samples increase, the crystallite sizes increase, whereas the residual strains in the nanoparticles slump. As it is known, the temperature can stimulate the atom's movement and cause an increase in the diffusion of atoms, resulting in crystallite growth. In addition, the atom's ability to move can reduce the saved strain in the lattice. The activation energy of crystallite growth (E) can be calculated according to Eq. (2) [23].

$$D = C\, exp((-E)/RT) \quad (2)$$

where D is the size of the crystallites, C is a constant, R is the gas constant, and T is the absolute calcination temperature. According to this equation, a straight line of $ln(D)$ against $1/T$ gives the activation energy of crystallite growth under the assumption that the growth of crystallites is homogenous (Fig. 6). The E value was calculated to be 43.2 KJ.mol^{-1}.

The morphology of the specimen heat treatment at 800 °C is shown in Fig. 7. As can be seen, the particles have an irregular form with an average particle size of 90 nm. In addition, some particles aggregate, forming large agglomerations. Two main reasons may cause such a coalescence of particles. First, the high surface energy of nanoparticles may render them to attach to each other to reduce their surfaces. Second, the magnetic nature of the cubic ferrite nanoparticles might create an attraction force that increases their adherence [24].

Fig. 8 presents the magnetization as a function of the applied field for specimens calcined at different temperatures. The measurements were carried out at room temperature. The hysteresis loops of the

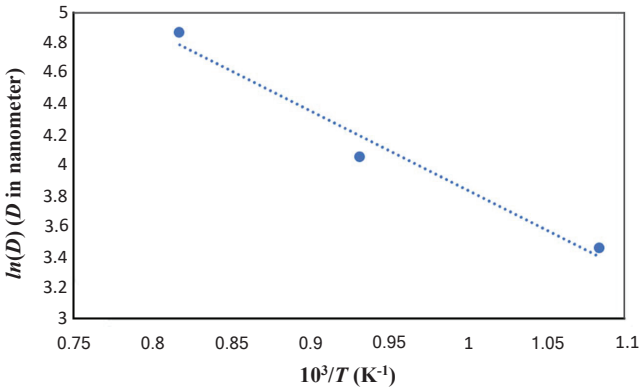

Fig. 6. Calculation of activation energy of crystallite growth, plotting $ln(D)$ versus $1/T$.

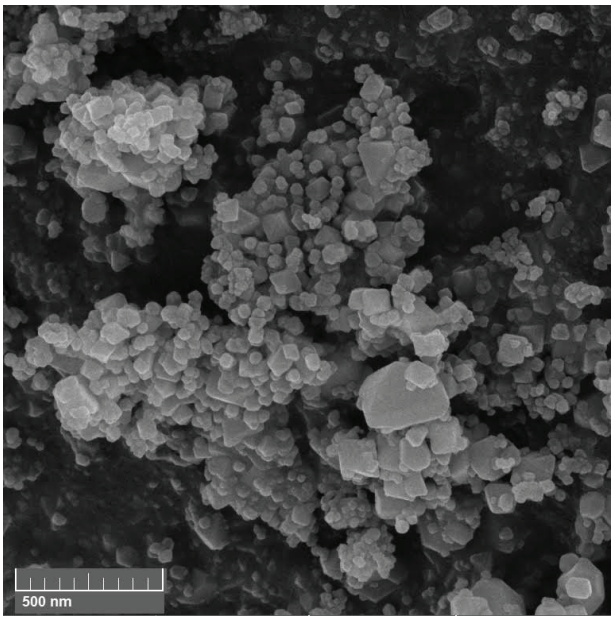

Fig. 7. SEM image of sample calcined at 800 °C.

samples are characteristic of soft magnetic materials, which have low coercivity. This feature is pertinent to ferromagnetic behavior.

The magnetic properties of the samples were calculated in Fig. 8 and presented in Fig. 9. As can be seen, the saturation magnetization (M_s) rises as the calcination temperature increases. The Ms of ferrites is dependent on different parameters, like the particle size, composition of the ferrite, the existence of dopants, etc. In the present work, the main reason for the increase in M_s is the rise of crystallite sizes, as shown in Fig. 5. It was reported that the greater surface of the smaller particles causes an increase in the disordering spin effect, which deteriorate magnetic properties. The coercivities of the sample show a slight decline with the rise of the calcination temperature [25]. The coercivity is also strongly affected by particle size. High permeability and low magnetic coercivity are necessary

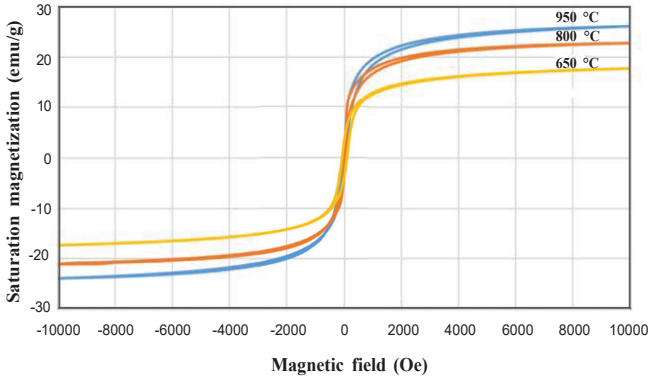

Fig. 8. Saturation magnetization versus the magnetic field.

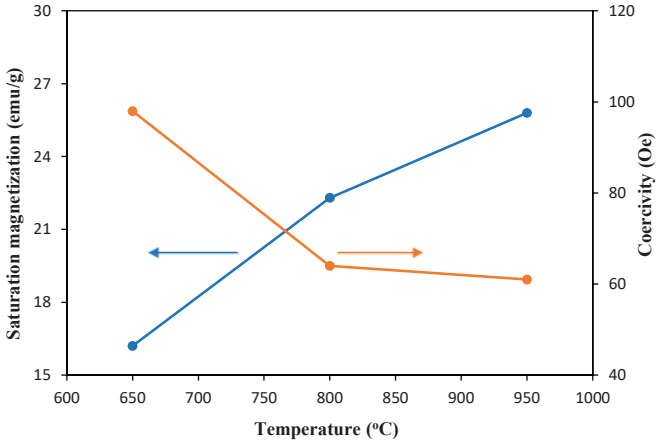

Fig. 9. Saturation magnetization and coercivity of samples against temperature.

for a soft magnetic material to be easily magnetized and demagnetized. In other words, coercivity should be as little as possible. The magnetic properties are affected by different variables, including microstrain, cation distribution, surface, magnetocrystalline, and shape anisotropies [26]. In addition, based on Ms, it is possible to understand the rise in coercivity values with increasing calcination temperature. Patange *et al.* reported that coercivity and saturation magnetization are related according to Eq. (3) (Brown's relation) [27].

$$\text{Coercivity} = (2k_1)/(\mu_0 M_s) \quad (3)$$

Through this equation, coercivity and saturation magnetization are connected so that coercivity is inversely proportional to M_s. Therefore, another reason for the reduction of coercivity may be an increase in M_s of samples that were heat-treated at higher temperatures.

4. Conclusions

In the present work, $NiFe_2O_4$ nanoparticles were fabricated via a polyacrylamide gel method with acrylamide, N,N'-methylene-bis-acrylamide, and ammonium persulfate as raw materials for polymeric gel agents. The fabricated nanoparticles were examined through FT-IR, STA, XRD, SEM, and VSM. The XRD results corroborated that the cubic nickel ferrites were successfully fabricated via the polyacrylamide gel method. The FT-IR and STA results showed that the volatile components and polymeric network were removed during calcination. The synthesized nanoparticles had irregular morphologies. The saturation magnetization and coercivity were strongly dependent

on calcination temperatures, so saturation magnetization increased by increasing the heat treatment temperature, whereas coercivity decreased.

Disclosure statement

No potential conflict of interest was reported by the author.

References

[1] Dippong, T., Levei, E.A., & Cadar, O. (2021). Recent advances in synthesis and applications of MFe_2O_4 (M = Co, Cu, Mn, Ni, Zn) nanoparticles. *Nanomaterials-Basel, 11*(6) 1560.

[2] Sharifianjazi, F., Moradi, M., Parvin, N., Nemati, A., Jafari Rad, A., Sheysi, N., Abouchenari, A., Mohammadi, A., Karbasi, S., Ahmadi, Z., Esmaeilkhanian, A., Irani, M., Pakseresht, A., Sahmani, S., & Shahedi Asl, M. (2020). Magnetic $CoFe_2O_4$ nanoparticles doped with metal ions: A review. *Ceram. Int. 46*(11) 18391-18412.

[3] Bouferrache, K., Charifi, Z., Baaziz, H., Alsaad, A.M., & Telfah, A. (2020). Electronic structure, magnetic and optic properties of spinel compound $NiFe_2O_4$. *Semicond. Sci. Tech. 35*(9) 095013.

[4] More, G.S., Shivhare, A., Kaur, S.P., Kumar, T.J.D., & Srivastava, R. (2022). Catalytic interplay of metal ions (Cu^{2+}, Ni^{2+}, and Fe^{2+}) in MFe_2O_4 inverse spinel catalysts for enhancing the activity and selectivity during selective transfer hydrogenation of furfural into 2-methylfuran. *Catal. Sci. Technol. 12*(15) 4857-4870.

[5] Li, D.-C., Muta, T., Zhang. L.-Q., Yoshio, M., & Noguchi, H. (2004). Effect of synthesis method on the electrochemical performance of $LiNi_{1/3}Mn_{1/3}Co_{1/3}O_2$. *J. Power Sources*, *132*(1-2)150-155.

[6] Ewais, E.M.M., Hessien, M.M., & El-Geassy, A.-H.A. (2008). *In-situ* synthesis of magnetic Mn-Zn ferrite ceramic object by solid state reaction. J. *Aust. Ceram. Soc. 44*(1) 57-62.

[7] Zahi, S., Daud, A.R., & Hashim, M. (2007). A comparative study of nickel-zinc ferrites by sol-gel route and solid-state reaction. *Mater. Chem. Phys. 106*(2-3) 452-456.

[8] Zhang, Z., Yao, G., Zhang, X., Ma, J., & Lin, H. (2015). Synthesis and characterization of nickel ferrite nanoparticles via planetary ball milling assisted solid-state reaction. *Ceram. Int. 41*(3) 4523-4530.

[9] Janasi, S.R., Emura, M., Landgraf, F.J.G., & Rodrigues, D. (2002). The effects of synthesis variables on the magnetic properties of coprecipitated barium ferrite powders. *J. Magn. Magn. Mater. 238*(2-3) 168-172.

[10] Komarneni S, D'Arrigo MC, Leonelli C, Pellacani, G.C., & Katsuki, H. (1998). Microwave-hydrothermal synthesis of nanophase ferrites. *J. Am. Ceram. Soc. 81*(11) 3041-3043.

[11] Deka, S., and Joy, P.A. (2006). Characterization of nanosized NiZn ferrite powders synthesized by an autocombustion method. *Mater. Chem. Phys. 100*(1) 98-101.

[12] Yue, Z., Guo, W., Zhou, J., Gui, Z. & Li, L. (2004). Synthesis of nanocrystilline ferrites by sol-gel combustion process: The influence of pH value of solution. *J. Magn. Magn. Mater. 270*(1-2) 216-223.

[13] Son. S., Taheri. M., Carpenter. E., Harris, V.G., & McHenry, M.E. (2002). Synthesis of ferrite and nickel ferrite nanoparticles using radio-frequency thermal plasma torch. *J. Appl. Phys. 91*(10) 7589-7591.

[14] Mohamed, R.M., Rashad, M.M., Haraz, F.A., & Sigmund, W. (2010). Structure and magnetic properties of nanocrystalline cobalt ferrite powders synthesized using organic acid precursor method. *J. Magn. Magn. Mater. 322*(14) 2058-2064.

[15] Pournajaf, R., and Hassanzadeh-Tabrizi, S.A. (2018). Polyacrylamide synthesis of nanostructured copper aluminate for photocatalytic application. *J. Adv. Mater. Process. 5*(4) 12-19.

[16] Quiroz, A., Chavira, E., Palomino-Merino, R., Guzmán, J., & Flores, C. (2022). Polymorphic synthesis and structural characterization of $NaSbO_3$ prepared by sol-gel acrylamide polymerization. *J. Solid State Chem. 315*, 123478.

[17] Sun, H., Bi, H., Jiang, C., Ni, Z., Tian, J., Zhou, W., Qiu, Z. & Lin, Q. (2022). Experimental study of the co-pyrolysis of sewage sludge and wet waste via TG-FTIR-GC and artificial neural network model: Synergistic effect, pyrolysis kinetics and gas products. *Renew Energ. 184*, 1-14.

[18] Che, H., Wu, Y., Wang, X., Liu, H., & Yan, M. (2023). Improved hydrogen storage properties of Li-Mg-NH system by lithium vanadium oxides. *J. Alloy. Compd. 931*, 167603.

[19] Ruxiang, Q., Liang, Z., Yu, G., & Youwei, H. (2021). Oxidation characteristics and active group

evolution of oil-immersed coal. *Environ. Earth. Sci. 80*, 433.

[20] Shi, J.-M., Zhang, X., Wu, C.-J., Shi, W., & Liu, L.-D. (2007). Synthesis, crystal structure and magnetic property of a one-dimensional copper (II) complex with 2, 5-dimethylpyrazine-1, 4-dioxide as bridging ligand. *J. Coord. Chem. 60*(17) 1827-1832.

[21] Jacintho, G.V.M., Brolo, A.G., Corio, P., Suarez, P.A.Z., & Rubim, J.C. (2009). Structural investigation of MFe_2O_4 (M= Fe, Co) magnetic fluids. *J. Phys. Chem. C, 113*(18) 7684-7691.

[22] Mustapha, S., Tijani, J.O., Ndamitso, M.M., Abdulkareem, A.S., Shuaib, D.T., Amigun, A.T. & Abubakar, H.L. (2021). Facile synthesis and characterization of TiO_2 nanoparticles: X-ray peak profile analysis using Williamson-Hall and Debye-Scherrer methods. *Int. Nano Lett. 11*, 241-261.

[23] Bouëxière, D., Popa, K., Walter, O., & Cologna, M. (2019). Kinetic study on the grain growth of PuO_2 nanocrystals. *RSC Adv. 9*, 6542-6547.

[24] Bernaoui, C.R., Bendraoua, A., Zaoui, F., Gallardo, J.J., Navas, J., Boudia, R.A., Djediai, H., Goual, N.H., & Adjdire, M. (2022). Synthesis and characterization of $NiFe_2O_4$ nanoparticles as reusable magnetic nanocatalyst for organic dyes catalytic reduction: study of the counter anion effect. *Mater. Chem. Phys. 292*, 126793.

[25] Shendruk, T.N., Desautels, R.D., Southern, B.W., & Van Lierop, J. (2007). The effect of surface spin disorder on the magnetism of γ-Fe_2O_3 nanoparticle dispersions. *Nanotechnology, 18*(45) 455704.

[26] Sun, L., Zhang, R., Wang, Z., Ju, L., Cao, E. & Zhang, Y. (2017). Structural, dielectric and magnetic properties of $NiFe_2O_4$ prepared via sol-gel auto-combustion method. *J. Magn. Magn. Mater. 421*, 65-70.

[27] Patange, S.M., Shirsath, S.E., Toksha, B.G., Jadhav, S.S., & Jadhav, K.M. (2009). Electrical and magnetic properties of Cr^{3+} substituted nanocrystalline nickel ferrite. *J. Appl. Phys. 106*(2) 023914.

Additional information

Correspondence and requests for materials should be addressed to S.A.H.T.

HOW TO CITE THIS ARTICLE

Hassanzadeh-Tabrizi, S.A. (2022). Synthesis, characterization, and magnetic properties of $NiFe_2O_4$ nanoparticles. *J. Particle Sci. Technol. 8(2) 79-85.*

DOI: 10.22104/JPST.2023.6046.1220

URL: https://jpst.irost.ir/article_1243.html